Steady-state traffic flow on a ring road with up- and down-slopes

Chun-Xiu Wu[a,b], Peng Zhang[a,d*], S.C. Wong[c], Keechoo Choi[e]

[a]Shanghai Institute of Applied Mathematics and Mechanics, Shanghai University, Shanghai, P.R. China

[b]College of Mathematics and Computer Science, Quanzhou Normal University, Quanzhou, Fujian Province, P.R. China

[c]Department of Civil Engineering, The University of Hong Kong, Pokfulam Road, Hong Kong SAR, P.R. China

[d]Shanghai Key Laboratory of Mechanics in Energy Engineering, Shanghai, P.R. China

[e]Department of Transportation Engineering, TOD-based Sustainable Urban Transportation Center, Ajou University, Suwon, Korea

Abstract: Steady-state traffic flow on a ring road with up- and down-slopes is investigated using a semi-discrete model. By exploiting the relations between the semi-discrete and continuum models, a steady-state solution is uniquely determined for a given total number of vehicles on a ring road. The solution is exact and always stable with respect to the first-order continuum model, whereas it is a good approximation with respect to the semi-discrete model provided that the involved equilibrium constant states are linearly stable. In other cases, the instability of one or more equilibria could trigger stop-and-go waves propagating in certain sections of road or throughout the ring road. The indicated results are reasonable and thus physically significant for better understanding of real-world traffic flow on inhomogeneous roads, such as those with junctions or bottlenecks.

Keywords: semi-discrete model; inhomogeneous road conditions; discontinuous fluxes; bottleneck; instability

*Corresponding author. E-mail: pzhang@mail.shu.edu.cn.

1 Introduction

In statistical physics, traffic flow has been viewed as a self-organized critical system [1, 2], and typical phases such as free flow, congestion, jamming together, and their transitions have been interpreted by a fundamental diagram (see [3] and references therein) and the three-phase theory [4,5]. More recently, traffic has been considered a coevolutionary process, and game theory has been used to depict driving behavior [6, 7]. As shown with the Biham-Middleton-Levine (BML) model [8], the choice between cooperation and defection exerts significant influence on the evolution of traffic states [6]. These theories were developed with large amounts of modeling and simulation assuming homogeneous road conditions (e.g., a single road with a uniform fundamental diagram).

In contrast, the influence of inhomogeneous road conditions (more generally those with bottlenecks or junctions) on traffic states has become a major concern in the development of traffic flow theory (e.g., see [3, 9]). In macroscopic modeling, the Riemann problem with discontinuous fluxes was studied mainly to design a numerical scheme that could be related to the theory of hyperbolic conservation laws with discontinuous fluxes [10–17]. In microscopic car-following modeling, steady-state flow over inhomogeneous sections of road was analytically or numerically studied by assuming or implying that the solution is a piecewise equilibrium constant in the inhomogeneous sections of road [18–23].

Such a steady-state solution can be described using the kinetic theory or the theory of hyperbolic conservation laws with discontinuous fluxes [14, 21], which is exact and stable for the first-order continuum Lighthill-Whitham-Richards (LWR) model [24,25]. However, it offers only an approximate solution to the car-following model or the higher-order model with relaxation if the relaxation time is sufficiently small; otherwise, it is unnecessarily stable due to the underlying metastability in these models. Nevertheless, this feature has not yet been well recognized or emphasized in the aforementioned studies of the car-following model.

In this context, the present paper addresses the problem using a semi-discrete model, which can be viewed as an extension of, and thus is more general than, the car-following model [26]. We enhance the mathematical analysis of steady-state flow on a ring road with up- and down-slopes, which poses more complexity for the solution. We also emphasize the instability of the solution with physical interpretation through the analysis of all equilibrium states and numerical simulation. Equilibrium traffic flow with an intermediate density value is widely regarded as unstable on a homogeneous ring road, which with oscillations is liable to evolve into stop-and-go waves (e.g., see [27–33]). Although the ring road discussed herein is much more complicated, and the simulation does not completely agree with the analytical results due to errors in the analysis, the steady-state solution is shown to have a similar tendency. That is, it is highly stable for large or small numbers of vehicles on

the ring road, and is unstable for intermediate numbers of vehicles. This result is important for understanding the macroscopic properties of traffic flow on an inhomogeneous road.

In Section 2 of this paper, the semi-discrete model and its correlation with the continuum model are discussed, and the linear stability condition for an equilibrium solution state is indicated. In Section 3, the wave pattern at a stationary interface is described using the theory of hyperbolic conservation laws with discontinuous fluxes, which helps to determine the two adjacent equilibrium constant states. Accordingly, the wave types of the steady-state solution on a ring road with up- and down-slopes, which depend on the total number of vehicles on the ring road, are indicated analytically. In Section 4, initial distributions with certain total numbers of vehicles are shown to converge to or diverge from the corresponding steady-state solutions through numerical simulation, which generally agrees with the analytical results. Concluding remarks are given in Section 5.

2 The semi-discrete model

In the semi-discrete model [26], a moving "particle" in traffic flow could be numbered by m with $x_m(t)$ being its position, and

$$\frac{dx_m(t)}{dt} = u_m(t),\ m = 0, \pm 1, \pm 2, \cdots \tag{1}$$

being its speed, and the acceleration can be defined through

$$\frac{d}{dt}[u_m(t) + p(s_m(t))] = \frac{1}{\tau}[u_e(s_m(t)) - u_m(t)]. \tag{2}$$

Here,

$$s_m(t) = [x_{m+1}(t) - x_m(t)]/\Delta M, \ \text{ and } \rho_m(t) \equiv (s_m(t))^{-1}, \tag{3}$$

are the specific volume and the density, respectively, represented by the particle m, ΔM is the mass between the particles m and $m+1$, and $u_e(s)$ and $p(s)$ are the equilibrium velocity-density relationship and the traffic pressure satisfying $u_e'(s) > 0$, and $p'(s) \leq 0$. For $\Delta M = 1$, the semi-discrete model of (1) and (2) reduces to a car-following model, in which case each particle can be viewed as a vehicle in that there is just one vehicle between the heads of two adjacent vehicles. The resulting car-following model is essentially the same as that in [31, 32, 34].

2.1 Correlation to the continuum model in Lagrange coordinates

Assume that there is no overtake between particles for division with a sufficiently small increment ΔM, and let M denote the total mass not passing through particle m. This implies that M referring

to particle m is independent of time t. Therefore, particle m can be identified by M and an associated variable $A_m(t)$ (e.g., the position $x_m(t)$ and speed $v_m(t)$) can be re-denoted by $A(M,t)$. Let $\Delta M \to 0$, then the flow can be viewed as a continuum in which M and t constitute the Lagrange coordinate system to describe the variable $A(M,t)$. In this case, Eq. (3) gives

$$s(M,t) = x_M(M,t), \quad \text{and } \rho(M,t) = (s(M,t))^{-1}. \tag{4}$$

Furthermore, we reduce Eq. (1) from $dx_{m+1}(t)/dt = u_{m+1}(t)$ and divide the resulting equation by ΔM. Then, for $\Delta M \to 0$, we have the following partially differential equation:

$$s_t(M,t) - u_M(M,t) = 0. \tag{5}$$

It is obvious that for $\Delta M \to 0$, Eq. (2) yields

$$[u(M,t) + p(s(M,t))]_t = \frac{u_e(s(M,t)) - u(M,t)}{\tau}. \tag{6}$$

The discussion implies the consistency between the semi-discrete model (1)-(2) and the continuum model (5)-(6), namely, the former system converges to the latter system for $\Delta M \to 0$.

2.2 Correlation to the continuum model in Euler coordinates

Let $A(M,t)$ now be denoted by the Euler coordinates (x,t) with $A(M,t) = A(x,t)$, where $x = x(M,t)$ is the position. We have

$$A_t(x,t) = A_x(x,t)x_t(M,t) + A_t(x,t), \ A_M(x,t) = A_x(x,t)x_M(M,t), \tag{7}$$

where $x_t(M,t) = u(M,t) = u(x,t)$, and $x_M(M,t) = s(M,t) = s(x,t) = 1/\rho(x,t)$, according to Eqs. (1) and (4). Replacing the partial derivatives of $s(M,t)$ and $u(M,t)$ in Eqs. (5)-(6) through Eq. (7), we have

$$\rho_t + (\rho u)_x = 0, \tag{8}$$

$$[\rho(u + P(\rho))]_t + [\rho u(u + P(\rho))]_x = \frac{\rho U_e(\rho) - \rho u}{\tau}, \tag{9}$$

where $P(\rho) = p(s)$, $U_e(\rho) = u_e(s)$, and $\rho = 1/s$. The system of (8)-(9) turns out to be the so called "anisotropic" higher-order traffic flow model [35–38]. This again establishes the correlation between the microscopic semi-discrete model and the macroscopic continuum model.

The consistency between the aforementioned three systems implies that the solution to the semi-discrete model should converge to the solution to the other two systems for $\Delta M \to 0$.

2.3 Stability of the equilibrium solution

An equilibrium constant state $(\rho_0, U_e(\rho_0))$ or $(s_0, u_e(s_0))$ is linearly stable with respect to the higher-order model (8)-(9) or (5)-(6) if

$$U_e'(\rho_0) + P'(\rho_0) \geq 0, \quad \text{or} \quad u_e'(s_0) + p'(s_0) \leq 0. \tag{10}$$

This corresponds to an equilibrium state

$$x_{m+1}^0(t) - x_m^0(t) = s_0 \Delta M, \text{ or } x_m^0(t) = u_e(s_0)t + m\Delta M s_0, \tag{11}$$

in the semi-discrete model (1)-(2), which is linearly stable if

$$u_e'(s_0) + p'(s_0) \leq \frac{\Delta M}{2\tau}. \tag{12}$$

As $\Delta M \to 0$, Eq. (12) reduces to Eq. (10), which also indicates the consistency between the continuum and the semi-discrete models. See [26] for a detailed discussion.

3 The steady-state solution over inhomogeneous sections of road

For discussion of the steady-state solution, the system (8)-(9) under the Euler coordinates is convenient for dealing with the interface between two inhomogeneous road sections. For a sufficiently small τ, Eq. (9) is approximated by $u = U_e(\rho)$, which together with Eq. (8) leads to the following LWR model [24, 25]:

$$\rho_t + (Q_e(\rho))_x = 0, \tag{13}$$

where $Q_e(\rho) = \rho U_e(\rho)$ is the flow-density relationship or fundamental diagram.

3.1 General discussion of the solution

In general, the steady-state solution $(\rho(x,t), u(x,t)) = (\rho(x), u(x))$ of (13) on an inhomogeneous road is piecewise constant, satisfying the equilibrium condition $u(x) = U_e(\rho(x))$. At each dividing point or interface, the flow $q \equiv \rho u = Q_e(\rho)$ is continuous and thus is constant over the entire road. However, density $\rho(x)$ and velocity $u(x)$ are usually discontinuous at the dividing point, which can be either a contact between two inhomogeneous sections of road or a stationary shock in a homogeneous section of road.

The constancy of the flow at the dividing point is attributed to the mass conservation or the Rankine-Hugoniot condition (see [11–14] and references therein). Let $\rho = \rho_{\mp}$ and $Q_e^{\mp}$ denote the

densities and the fundamental diagrams on the left and the right sides of the interface. Then, the mass conservation is simply that

$$Q_e^-(\rho_-) = Q_e^+(\rho_+). \tag{14}$$

For the dividing point that is stationary, a "wave entropy" condition can be applied at the interface to describe valid wave breaking on both sides [11–14]. That is, the characteristic speeds on the two sides take the same sign with

$$(Q_e^-(\rho_-))'(Q_e^+(\rho_+))' > 0. \tag{15}$$

Otherwise, we have

$$(Q_e^+(\rho_+))' \geq 0, \text{ if } (Q_e^-(\rho_-))' = 0; \tag{16}$$

and

$$(Q_e^-(\rho_-))' \leq 0, \text{ if } (Q_e^+(\rho_+))' = 0. \tag{17}$$

See also [15, 16] for a similar entropy condition.

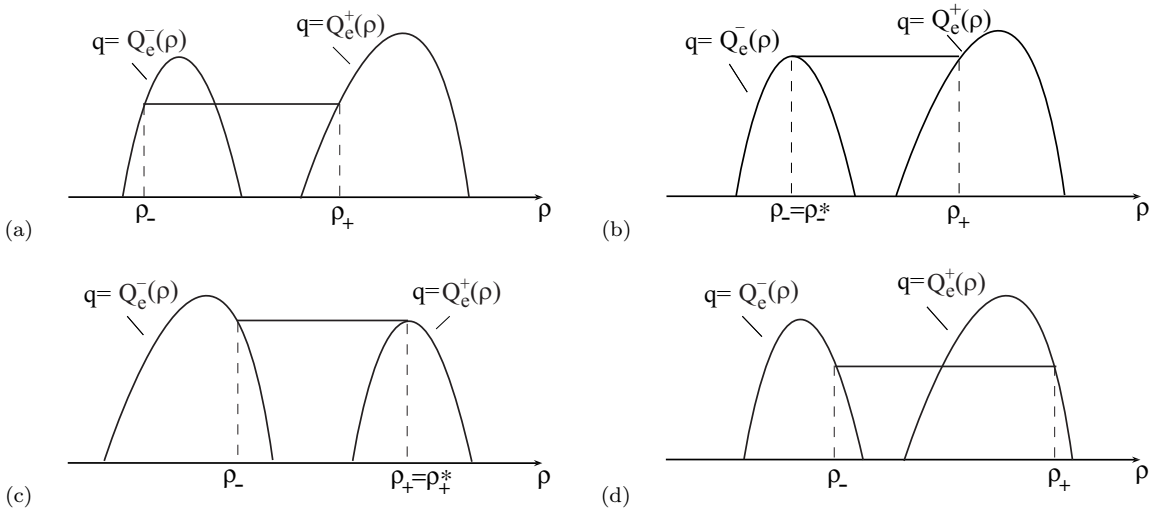

Fig. 1 Four wave patterns at a joint, obeying the conservation of (14), such that the outflow $Q_e^-(\rho_-)$ equals the inflow $Q_e^+(\rho_+)$, where $Q_e^\mp(\rho)$ are the fundamental diagrams on the upstream and downstream road sections. (a) and (d): normal and congested wave patterns associated with Eq. (15); (b) and (c): wave patterns with upstream and downstream traffic at capacity associated with Eqs. (16) and (17). These help determine $\rho_\pm$.

We assume that the critical densities are ρ_-^* and ρ_+^* with $Q_e(\rho_-^*)$ and $Q_e(\rho_+^*)$ being the maximal flows or capacities on the left- and the right-hand sides, i.e.,

$$(Q_e^{\mp}(\rho_{\mp}^*))' = 0,\ (\rho - \rho_{\mp}^*)(Q_e^{\mp}(\rho))' < 0,\ \text{for } \rho \neq \rho_{\mp}^*. \tag{18}$$

For the discussed steady-state solution $\rho = \rho(x)$, we obviously have

$$Q_e(\rho(x)) \leq \min(Q_e^-(\rho_-^*), Q_e^+(\rho_+^*)), \tag{19}$$

and the term on the right-hand side is defined as the capacity with respect to the two divided sections. Thus, we have four wave patterns at the interface (Fig. 1). The normal and the congested wave patterns (Figs. 1(a) and (d), respectively) are associated with Eq. (15). Wave patterns with upstream and downstream traffic at capacity (Fig. 1(b) and (c), respectively) are associated with Eq. (16) and (17) and occur only if $Q_e^-(\rho_-^*) \leq Q_e^+(\rho_+^*)$ or vice versa. We call the interface a bottleneck if $Q_e^-(\rho_-^*) > Q_e^+(\rho_+^*)$, which triggers a queue upstream from the interface when the traffic downstream is at capacity.

3.2 The solution on a ring road with up- and down-slopes

Steady-state flow on an inhomogeneous highway road is characterized by the wave pattern at each of the interfaces. For a road with up- and down-slopes, we adopt the following velocity-specific volume relationship:

$$u_e(s) = \frac{u_f(\beta)[tanh(s/l - x_c(\beta)/l) + tanh(x_c(\beta)/l - 1)]}{1 + tanh(x_c(\beta)/l - 1)}, \tag{20}$$

where β is the slope, l the vehicle length, and $u_f(\beta)$ the free-flow velocity. We can easily see that $u_e(l) = 0$, $u_e(+\infty) = u_f(\beta)$, and $u_e'(s) > 0$, for $s \geq l$. By the relations $U_e(\rho) = u_e(s)$, $\rho = s^{-1}$, we correspondingly have $U_e'(\rho) < 0$, for $\rho \in [0, \rho_{jam}]$, and $U_e(\rho_{jam}) = 0$, $U_e(0) = u_f(\beta)$, where $\rho_{jam} = 1/l$ is the jamming density. By scaling, the free-flow velocity $u_f(\beta)$ and the safe interval $x_c(\beta)$ are determined by the following piecewise functions:

$$\frac{u_f(\beta)}{u_f(0)} = \begin{cases} -100\beta^2 - 5\beta + 1, & -0.10 \leq \beta < 0, \\ 1, & 0 \leq \beta < 0.02, \\ -150\beta^2 + 3\beta + 1, & 0.02 \leq \beta \leq 0.08, \\ 0.28, & 0.08 < \beta \leq 0.10, \end{cases} \quad u_f(0) = 30\ m/s, \tag{21}$$

and

$$\frac{x_c(\beta)}{l} = \begin{cases} 300\beta^2 - 12\beta + 3, & -0.10 \leq \beta < 0, \\ 80\beta^2 + 15\beta + 3, & 0 \leq \beta \leq 0.10, \end{cases} \quad l = 4.5\ m, \tag{22}$$

The formula (20) is extended from that in [32], and Eqs. (21)-(22) are based on the experimental study in [39]. The formula (20) can also be viewed as a modification of that in [22], which was extended from that in [40]. We note that the properties of (18) can be verified for $|\beta| \leq 0.1$.

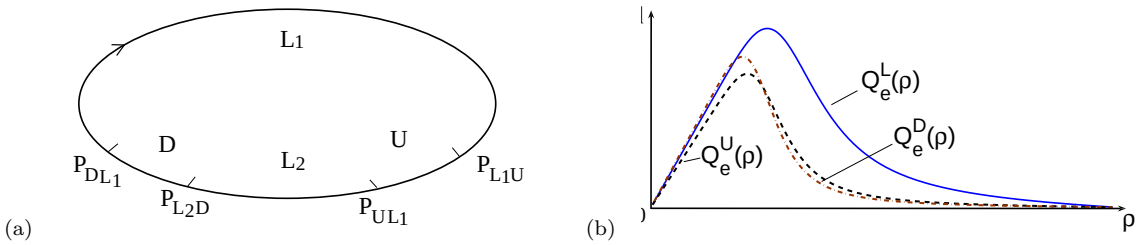

Fig. 2 (a) The clockwise ring road $R = L_1 \cup U \cup L_2 \cup D$, with the lengths $|R| = 6750m$, $|L_1| = 4050m$, $|U| = 675m$, and $|D| = 675m$; (b) the fundamental diagrams $q = Q_e^L(\rho)$, $q = Q_e^U(\rho)$, and $q = Q_e^D(\rho)$, for the level road sections $L_1 \cup L_2$, the up-slope section U, and the down-slope section D, respectively, which are defined through Eqs. (20)-(22).

We now consider a clockwise ring road R which is composed of four sections: (i) the level road L_1 with $\beta = 0$; the up-slope U with $\beta = 0.04$; the level road L_2 with $\beta = 0$; and the down-slope D with $\beta = -0.04$. The joints between two adjacent sections are denoted by P_{L_1U}, P_{UL_2}, P_{L_2D}, and P_{DL_1}. The ring road is shown in Fig. 2(a), and the fundamental diagrams $q = Q_e(\rho)$ for all sections are shown in Fig. 2(b). We see that by Fig. 2(b),

$$Q_s \leq \min(Q_e^L(\rho_L^*), Q_e^U(\rho_U^*), Q_e^D(\rho_D^*)) = Q_e^U(\rho_U^*) \equiv Q_c, \tag{23}$$

where $Q_s = Q_e(\rho(x))$ is the flow corresponding to the steady-state solution $\rho(x)$, and Q_c is defined as the capacity of the ring road. Eq. (23) is the extension of Eq. (19). Given Q_s, we have two solution values of $\rho(x)$ through Eqs. (20)-(22). However, $\rho(x)$ can be uniquely determined according to the wave pattern at each dividing point. In fact, Q_s together with the wave patterns can be uniquely determined by the total number N of vehicles on the ring road, which is indicated in the following discussion by referring to Figs. 2(a) and (b).

For N increasing from $N = 0$, Q_s increases until it reaches capacity with $Q_s = Q_c$, when the total number of vehicles

$$N_{t_1} = \sum_{\chi} |\chi| \rho_\chi, \ \chi = L_1, U, L_2, D. \tag{24}$$

Here, $|\chi|$ and ρ_χ represent the lengths of and the densities in the four sections divided by P_{L_1U}, P_{UL_2}, P_{L_2D}, and P_{DL_1}. In this case, we have $\rho_\chi < \rho_\chi^*$, except for $\rho_U = \rho_U^*$.

For $N < N_{t_1}$, we have $Q_s < Q_c$, and $\rho_\chi < \rho_\chi^*$, for all χ, and thus the interfaces at all dividing points represent normal wave patterns, which are associated with Eqs. (11)-(12). Accordingly, the

constant flow Q_s together with the densities ρ_χ in the four sections is uniquely determined by

$$\sum_\chi |\chi|\rho_\chi = N,\ Q_e(\rho_\chi) = Q_s,\ \chi = L_1, U, L_2, D. \tag{25}$$

For $N > N_{t_1}$, we have the same flow rate $Q_s = Q_c$ and other density values as in the case of $N = N_{t_1}$, except for a "blow-up" upstream from P_{L_1U}, which is due to the capacity drop $Q_e(\rho_U^*) = Q_c < Q_e(\rho_L^*)$ (see Eq. (23) and Fig. 2(b)) at this interface. According to the discussion in Section 3.1, this suggests that P_{L_1U} represent the one and only bottleneck on the whole road with respect to the discussed solution. In this case, L_1 is divided into two intervals L_{11} and L_{12}, and their lengths together with the dividing point are determined by N through the following equation:

$$N = \sum_\chi |\chi|\rho_\chi,\ \chi = L_{11}, L_{12}, U, L_2, D. \tag{26}$$

In this case, the traffic is downstream capacitated at P_{L_1U}, and $P_{L_{11}L_{12}}$ represents the position P_s of a stationary shock; the threshold value of N is computed by

$$N_{t_2} = \sum_\chi |\chi|\rho_\chi,\ \chi = L_1, U, L_2, D, \tag{27}$$

when P_s coincides with P_{DL_1}.

As N continues to increase, the position P_s of the stationary shock moves upstream until it reaches the joint P_{UL_2}, which is between the up-slope and level road 2. In this process, a joint comes to represent a congested wave pattern if its position is downstream from P_s. We have the threshold value

$$N_{t_3} = \sum_\chi |\chi|\rho_\chi,\ \chi = L_1, U, L_2, D, \tag{28}$$

when P_s coincides with P_{L_2D}, and the threshold value

$$N_{t_4} = \sum_\chi |\chi|\rho_\chi,\ \chi = L_1, U, L_2, D, \tag{29}$$

when P_s coincides with P_{UL_2}. The solution $\rho(x)$ together with the position P_s of the stationary shock for N between N_{t_i} and $N_{t_{i+1}}$ $(i = 2, 3)$ can be determined similarly to Eq. (26).

For $N > N_{t_4}$, the constant flow Q_s cannot reach the capacity Q_c of the ring road. As N increases, Q_s begins to decrease until $Q_s = 0$, when the whole road becomes completely blocked. With this development, Q_s together with ρ_χ in the four sections is determined also by Eq. (25), except that each joint between two adjacent road sections represents a congested wave pattern.

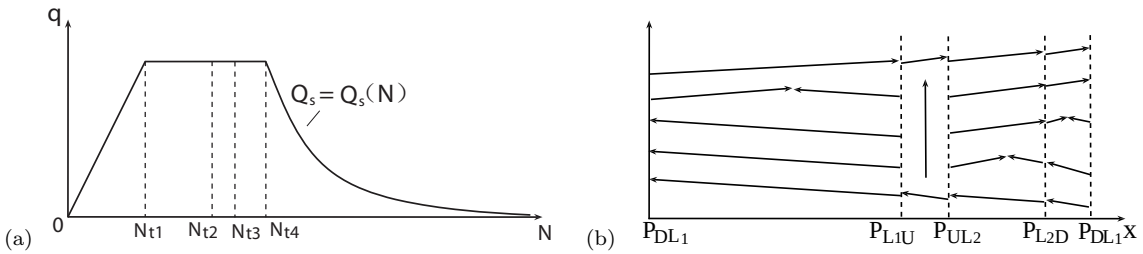

Fig. 3 (a) Steady-state flow rate in relation to the total number of vehicles: $Q_s = Q_s(N)$; (b) wave patterns corresponding to the cases of $N < N_{t_1}$, $N_{t_1} < N < N_{t_2}$, $N_{t_2} < N < N_{t_3}$, $N_{t_3} < N < N_{t_4}$, and $N > N_{t_4}$, from the top to bottom, respectively, where "↗", "↑", and "↘" denote that the directions of characteristics are forward ($Q_e'(\rho) > 0$), stationary ($Q_e'(\rho) = 0$), and backward ($Q_e'(\rho) < 0$).

The function $Q_s = Q_s(N)$ is shown in Fig. 3(a). Corresponding to all discussed cases, the wave patterns at all joints together with the characteristic speeds $dx/dt \equiv Q_e'(\rho)$ in all sections are shown in Fig. 3(b).

4 Numerical simulation

The semi-discrete model of (1)-(2) is used for numerical simulation. We casually set the following initial distribution:

$$s_0 = \frac{|R|}{N},\ x_m(0) = ms_0,\ v_m(0) = u_e(s_0),\ m = 1, \cdots, N, \tag{30}$$

and define $s_N(t) = (x_1(t) + |R| - x_N(t))/\Delta M$ in Eq. (2), where the length of the ring road $|R| = 6750m$. In the simulation, the position that is 2700 meters downstream from the joint P_{L_1U} is taken as the origin. Moreover, the length of a road section is scaled by $l = 4.5m$ and the density is scaled by $\rho_{jam} = 1/l$. As a consequence, the coordinates of the joints P_{L_1U}, P_{UL_2}, P_{L_2D}, and P_{DL_1} are 600, 750, 1050, and 1200, respectively.

Because $u_e(s_0)$ in Eq. (30) depends on the slope β, the vehicular velocities in different sections of road are not equal. As a consequence, the headway cannot remain constant as the traffic conditions evolve. Then, given the total number N of vehicles on the ring road, the simulation is designed to test whether the initial distribution of Eq. (30) converges to the corresponding steady-state solution. Because the simulation involves a stiff relaxation with small τ, a semi-implicit scheme for time discretization of (1)-(2) is adopted,

$$\frac{x_m^{(n+1)} - x_m^{(n)}}{\Delta t} = u_m^{(n)},\ \ \frac{u_m^{(n+1)} + p(s_m^{(n+1)}) - u_m^{(n)} - p(s_m^{(n)})}{\Delta t} = \frac{u_e(s_m^{(n)}) - u_m^{(n+1)}}{\tau}, \tag{31}$$

where $s_m^{(n)} = x_{m+1}^{(n)} - x_m^{(n)}$.

The convergence or divergence is actually associated with the stability or instability of the discussed steady-state solution, for which the linear stability condition of (12) for the involved equilibrium states is referred to for comparison. However, we should note that not all lengths of these equilibrium states are adequate to apply Eq. (12) and that the coupling effect between two adjacent equilibrium states is neglected. Moreover, the perturbation arising from (30) to the corresponding steady-state solution can be hardly regarded as "small". These factors should give rise to considerable errors in the comparison.

Table 1 Comparison between equilibrium values of the steady-state solution and simulated mean values of the semi-discrete model on the divided sections. The initial distribution of Eq. (30) always converges to the steady-state solution for sufficiently small relaxation times ($\tau = 0.03s$), whereas it may diverge from the steady-state solution for large relaxation times ($\tau = 0.3s$), which bring about unstable equilibrium states of the solution.

	analytical equilibrium values				simulated with $\tau = 0.03s$				simulated with $\tau = 0.3s$			
N	L_1	U	L_2	D	L_1	U	L_2	D	L_1	U	L_2	D
250	.1610	.2228	.1610	.1557	.1633	.2000	.1633	.1600	.1633	.2000	.1633	.1600
330	.1644	.2080	.1644	.1592	.1648	.2133	.1633	.1600	.1670	.2000	.1633	.1600
	.3329				.3326				.3348			
420	.3329	.2080	.1644	.2297	.3322	.2067	.1667	.2333	.3333	.2000	.1778	.2133
			.3329				.3333				.3333	
550	.3906	.2749	.3906	.2667	.3911	.2733	.3900	.2667	.4111	.2667	.3433	.2467
620	.4418	.3061	.4418	.2930	.4400	.3067	.4433	.3000	.5089	.2133	.3267	.2133
675	.4824	.3285	.4824	.3124	.4833	.3267	.4767	.3200	.4833	.3267	.4800	.3133

We choose $\Delta M = 1$ to implement a realistic car-following simulation, in which case particle m represents a vehicle and $s_m(t)$ is the headway between vehicles m and $m+1$. Even if ΔM is not so small, we show that the convergence for τ is sufficiently small to ensure the stability condition of (12) for all s_0. Table 1 shows sets of simulated mean density values for comparison with the equilibrium density values of the corresponding steady-state solution discussed in Section 3.1. The simulation results are also shown in Fig. 4, by which we clearly observe the convergence. In this case, the semi-discrete model together with its full discrete form of (31) works similarly to a relaxation scheme for solving the LWR model of (13) (see [41–43] for detailed discussion of the relaxation scheme).

However, it is more physically significant to deal with unstable traffic flow in the ring road by taking a much larger relaxation time, by which Eq. (12) suggests a narrower region of s_0 for the stability of the involved equilibrium states. We take $\tau = 0.3s$, which is more realistic when compared with the values that are widely used for the car-following model in the literature. With the same values of N, the simulated mean values are also given in Table 1, and the simulation results are also

shown in Fig. 4 to observe the convergence or divergence.

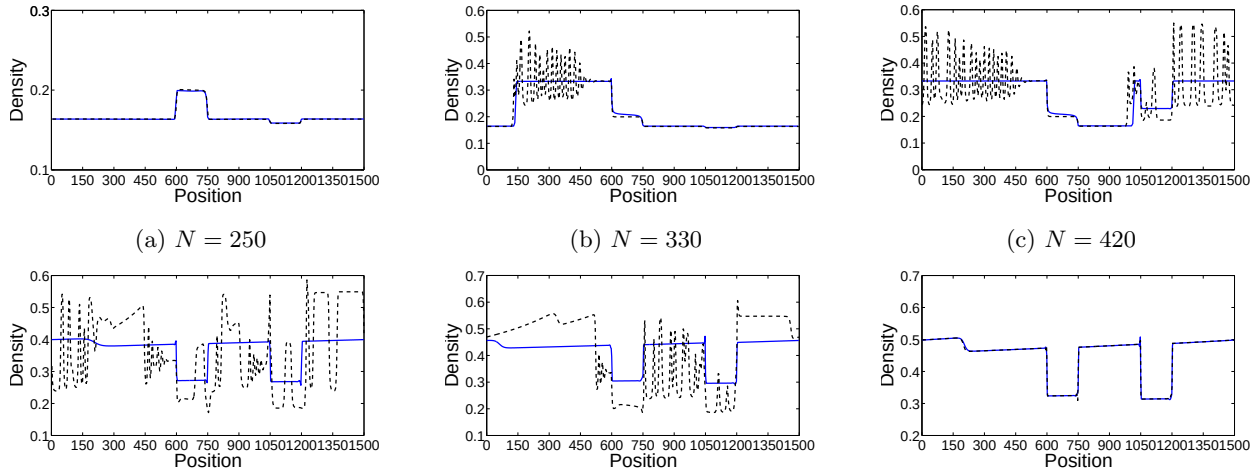

(a) $N = 250$ (b) $N = 330$ (c) $N = 420$

(d) $N = 550$ (e) $N = 620$ (f) $N = 675$

Fig. 4 Density distributions for different total numbers N of vehicles at $t = 1500s$, which are evolved from the initial distribution of Eq. (30). For a sufficiently small relaxation time $\tau = 0.03s$, the traffic is generally quite stable (solid blue line). For a much larger and more realistic relaxation time $\tau = 0.3s$ (dotted black line), the traffic is stable for N that is small or large but unstable for intermediate values of N.

Table 2 Changes in solution properties arising from changes in N. The second column shows the monotone change of $Q_s = Q_s(N)$, where the threshold values $N_{t_1} = 253$, $N_{t_2} = 404$, $N_{t_3} = 415$, and $N_{t_4} = 466$ are determined by Eqs. (21) and (23)-(26) (also compare with Fig. 3). Other columns show the stability (S) or instability (I) of the involved equilibrium states by using Eq. (29) with $\tau = 0.3s$.

N	Q_s	L_1	U	L_2	D
$[0, 253]$	$\nearrow$	S	S	S	S
$(253, 404)$	$= Q_c$	(S, I)	S	S	S
$[404, 415)$	$= Q_c$	I	S	S	(S, I)
$[415, 466)$	$= Q_c$	I	S	(S, I)	I
$[466, 478]$	$\searrow$	I	S	I	I
$(478, 579)$	$\searrow$	I	I	I	I
$[579, 637)$	$\searrow$	S	I	S	I
$[637, 657)$	$\searrow$	S	S	S	I
$[657, 1500]$	$\searrow$	S	S	S	S

All involved equilibrium states and their stability (for $\tau = 0.3s$) depend on the total number N of vehicles on the ring road, which is again taken as a characteristic parameter, and of which the threshold values for changes in stability are combined with those in Eqs. (24) and (27)-(29) to

further classify the solution (see also Fig. 3). Table 2 indicates the solution properties, especially the stability (S) or instability (I) of the equilibrium states with respect to the semi-discrete model, which is according to Eq. (12).

Table 2 agrees with Fig. 4 except for some inconsistency in the stability of the equilibrium states of the semi-discrete model, which corresponds to Fig. 4(e). However, both Table 2 and Fig. 4 indicate a similar tendency. That is, the whole solution is quite stable and convergent to the steady-state solution for small or large N; the occurrence of instability becomes frequent and intensive for intermediate values of N. This tendency is similar to (but is more complex than) that for a homogeneous, level ring road, which was indicated by both theoretical and experimental studies [27–30, 44].

Most oscillations in Figs. 4(b)-(e) represent stop-and-go waves in traffic. Among these, the waves in Figs. 4(b)-(c) demonstrate propagations only within one or more road sections, whereas we observe steady-state traffic flow in other road sections through comparison with the simulated results for $\tau = 0.03s$. In contrast, the waves in Figs. 4(d)-(e) propagate throughout the ring road, in which case no steady states are observed locally. However, we see some regularity in the backward moving stop-and-go waves, which are somewhat similar to (but not as regular as) those traveling waves that were studied under homogeneous ring road conditions [26–29, 32]. Fig. 5 shows the evolution process for $N = 550$, which corresponds to Fig. 4(d).

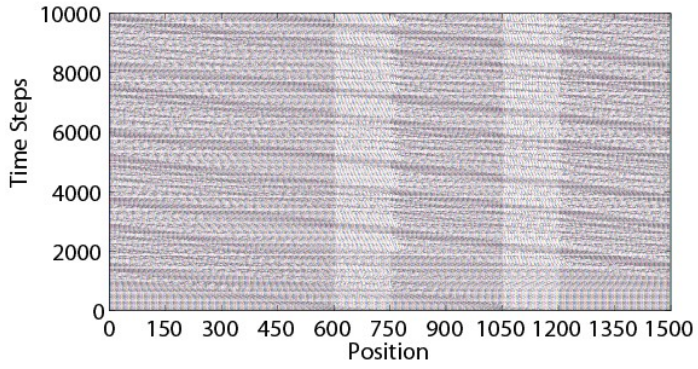

Fig. 5 Evolution of the initial distribution of Eq. (30), with $N = 550$, and 10000 time steps (for $t \leq 1500s$). Stop-and-go waves are observed moving backward throughout the ring road.

5 Conclusions

We thoroughly investigated the steady-state solution on an inhomogeneous ring road using a semi-discrete model and uniquely determined the steady-state solution according to the analysis of the wave pattern at a dividing point between two equilibria. Moreover, the stability of the solution was

related to that of the involved equilibria.

We found that both the wave types and the stability of the steady-state solution depend on the total number N of vehicles on the ring road and that the simulation results agree with the analysis in general. For the case with a realistic relaxation time $\tau = 0.3s$, a casually distributed traffic state (of Eq. (30)) can stably evolve into the corresponding steady-state flow for light or heavy traffic with small or large number N of vehicles but is liable to generate stop-and-go waves for congested traffic with intermediate values of N. This tendency is similar to that found on a homogeneous, level ring road, and the indicated phenomena are physically significant for the better understanding and management of traffic flow on an inhomogeneous road in general. However, at least two issues are left for future study.

1. More efficient tools are required for stability analysis of the discussed steady-state solution due to the inadequate lengths and the neglect of interaction between the involved equilibrium states in the current analysis.

2. Multi-lane traffic should be taken into account to present more realistic scenarios. Under the framework of the present paper, the traffic flow in each lane would be described separately except for the interaction between two adjacent lanes. In this case, formulation of a lane-change maneuver should be physically sound (e.g., to reflect cooperation and defection as was done in [6] using the BML model [8]). However, assignment of traffic flow (the Riemann solution) at a link between two or more sections of road would pose a difficult problem for such modeling (e.g., see the discussion in [45]).

Acknowledgements

This study was jointly supported by grants from the National Natural Science Foundation of China (11072141), the National Basic Research Program of China (2012CB725404), the Shanghai Program for Innovative Research Team in Universities, the Research Grants Council of the Hong Kong Special Administrative Region, China (Project No. HKU7188/11E), a National Research Foundation of Korea grant funded by the Korean government (MEST) (NRF-2010-0029446), and the Scientific Research Foundation for the Talents of Quanzhou Normal University.

References

[1] D. Helbing, Traffic and related self-driven many-particle systems, Rev. Mod. Phys., 73 (2001) 1067-1141.

[2] C. Leduc, K. Padberg-Gehle, V. Varga, D. Helbing, S. Diez, J. Howard, Molecular crowding creates traffic jams of kinesin motors on microtubules, PNAS 109 (2012) 6100-6105.

[3] A. Mazloumian, N. Geroliminis, D. Helbing, The spatial variability of vehicle densities as determinant of urban network capacity, Phil. Trans. R. Soc. A 368 (2010) 4627-4647.

[4] B.S. Kerner, Introduction of Modern Traffic Flow Theory and Control, Springer, Berlin, New York, 2009.

[5] B.S. Kerner et al., Traffic dynamics in empirical probe vehicle data studied with three-phase theory: Spatiotemporal reconstruction of traffic phases and generation of jam warning messages, Physica A 392 (2013) 221-251.

[6] M. Perc, Premature seizure of traffic flow due to the introduction of evolutionary games, New J. Phys., 9 (2007) 1-17.

[7] M. Perc, A. Szolnoki, Coevolutionary games-A mini review, BioSystems 99 (2010) 109-125.

[8] O. Biham, A.A. Middleton, D. Levine, Self organization and a dynamical transition in traffic flow models, Phys. Rev. A 46 (1992) R6124.

[9] I. Gasser, B. Werner, Dynamical phenomena induced by bottleneck, Phil. Trans. R. Soc. A 368 (2010) 4543-4562.

[10] W. Jin, H.M. Zhang, The inhomogeneous kinematic wave traffic flow model as a resonant nonlinear system, Transport. Sci. 37 (2003) 294-311.

[11] P. Zhang, R.X. Liu, Hyperbolic conservation laws with space-dependent flux: I Characteristics theory and Riemann problem, J. Comput. Appl. Math. 156 (2003) 1-21.

[12] P. Zhang, R.X. Liu, S.C. Wong, High-resolution numerical approximation of traffic flow problems with variable lanes and free flow velocities, Phys. Rev. E 71 (2005) 056704.

[13] P. Zhang, S.C. Wong, Z.L. Xu, A hybrid scheme for solving a multi-class traffic flow model with complex wave breaking, Comput. Methods Appl. Mech. Engrg., 197 (2008) 3816-3827.

[14] P. Zhang, D.Y. Wu, S.C. Wong, Y.Z. Tao, Kinetic description of bottleneck effects in traffic flow, Appl. Math. Mech. (-English Ed.) 30 (2009) 425-434.

[15] R. Bürger, A. Gracía, K.H. Karlsen, J.D. Towers, A family of numerical schemes for kinematic flows with discontinuous flux, J. Eng. Math. 60 (2008) 387-425.

[16] R. Bürger, A. Gracía, K.H. Karlsen, J.D. Towers, Difference schemes, entropy solutions, and speedup impulse for an inhomogeneous kinematic traffic flow model, Netw. Heterog. Media 3 (2008) 1-41.

[17] W.J. Sun, S.C. Wong, P. Zhang, C.-W. Shu, Shock-fitting algorithm for the LWR model on inhomogeneous highways, Transportmetrica 7 (2011) 163-180.

[18] R. Nagai, H. Hanaura, K. Tanaka, T. Nagatani, Discontinuity at edge of traffic jam induced by slowdown, Physica A 364 (2006) 464-472.

[19] K. Tanaka, H. Hanaura, T. Nagatani, Traffic jam and discontinuity induced by slowdown in two-stage optimal-velocity model, Physica A 370 (2006) 756-768.

[20] H. Hanaura, T. Nagatani, K. Tanaka, Jam formation in traffic flow on a highway with some slowdown sections, Physica A 374 (2007) 419-430.

[21] J. Ward, R.E. Wilson, P. Berg, Multiscale analysis of a spatially heterogeneous microscopic traffic model, Physica D 236 (2007) 1-12.

[22] X.L. Li, T. Song, H. Kuang, S.Q. Dai, Phase transition on speed limit traffic with slope, Chinese Phys. B 17 (2008) 3014-3020.

[23] H.D. He, W.Z. Lu, Y. Xue, L.Y. Dong, Dynamic characteristics and simulation of traffic flow with slope, Chinese Phys. B 18 (2009) 2703-2708.

[24] M.J. Lighthill, G.B. Whitham, On kinematic waves: II. A theory of traffic flow on long crowded roads, Proc. Roy. Soc. London, Ser. A 229 (1955) 317-345.

[25] P.I. Richards, Shockwaves on the highway, Oper. Res. 4 (1956) 42-51.

[26] P. Zhang, C.X. Wu, S.C. Wong, A semi-discrete model and its approach to a solution for wide moving jam in traffic flow, Physica A 391 (2012) 456-463.

[27] B. S. Kerner, P. Konhauser, Structure and parameters of clusters in traffic flow, Phys. Rev. E 50 (1994) 54-83.

[28] P. Zhang, S.C. Wong, Essence of conservation forms in the traveling wave solutions of Higher-Order Traffic Flow Model, Phys. Rev. E 74 (2006) 026109.

[29] R.Y. Xu, P. Zhang, S.Q. Dai, S.C. Wong, Admissibility of a wide cluster solution in "anisotropic" higher-order traffic flow models, SIAM J. Appl. Math. 68 (2007) 562-573.

[30] W.L. Jin, H.M. Zhang, The formation and structure of vehicle clusters in the Payne-Whitham traffic flow model, Transp. Res. B 37 (2003) 207-223.

[31] J. Greenberg, Extensions and amplifications of a traffic model of Aw and Rascle, SIAM J. Appl. Math. 62 (2001) 729-745.

[32] J.M. Greenberg, Congestion redux, SIAM J. Appl. Math. 64 (2004) 1175-1185.

[33] D. Ngoduy, Platoon-based macroscopic model for intelligent traffic flow, Transportmetrica B: Transport Dynamics, 1(2) (2013) 153-169.

[34] A. Aw, A. Klar, T. Materne, M. Rascle, Derivation of continuum traffic flow models from microscopic follow-the-leader models, SIAM J. Appl. Math. 63 (2002) 259-278.

[35] A. Aw, M. Rascle, Resurrection of "second order" models of traffic flow, SIAM J. Appl. Math. 60 (2000) 916-938.

[36] M. Rascle, An improved macroscopic model of traffic flow: Derivation and links with the Lighthill-Whitham model, Math. Comput. Model. 35 (2002) 581-590.

[37] H.M. Zhang, A non-equilibrium traffic model devoid of gas-like behavior, Transp. Res. B 36 (2002) 275-290.

[38] H.M. Zhang, Comment on "On the controversy around Daganzo's requiem for and Aw-Rascle's resurrection of second-order traffic flow models" by D. Helbing and A.F. Johansson, Eur. Phys. J. B 69 (2009) 563-568.

[39] R.G. Zhou, L.S. Jiang, J.F. Sun, The study of highway gradient and grade length limit, J. Highway Transp. Res. Dev. 21 (7) (2004).

[40] M. Bando, K. Hasebe, A. Nakayama, A. Shibata, Y. Sugiyama, Dynamical model of traffic congestion and numerical simulation, Phys. Rev. E 51 (1995) 1035-1042.

[41] S. Jin, Z.P. Xin, Numerical passage from systems of conservation laws to Hamilton-Jacobi equations, and relaxation schemes, SIAM J. Numer. Anal. 35 (1998) 2385-2404.

[42] S. Jin, L. Pareschi, G. Toscani, Uniformly accurate diffusive relaxation schemes for multiscale transport equations, SIAM J. Numer. Anal. 38 (2000) 913-936.

[43] M. Herty, L. Pareschi, M. Seaid, Discrete-velocity models and relaxation schemes for traffic flows, SIAM J. Sci. Comput. 28 (2006) 1582-1596.

[44] Y. Sugiyama et al., Traffic jams without bottlenecks-experimental evidence for the physical mechanism of the formation of a jam, New J. Phys. 10 (2008) 033001.

[45] B. Schnetzler, X. Louis, J.P. Lebacque, A multilane junction model, Transportmetrica, 8(4) (2012) 243-260.